OMTN, Volume *32*

Supplemental information

LncRNA ZNF593-AS alleviates diabetic cardiomyopathy via suppressing IRF3 signaling pathway

Rong Xie, Jiahui Fan, Jianpei Wen, Kunying Jin, Jiabing Zhan, Shuai Yuan, Yuyan Tang, Xiang Nie, Zheng Wen, Huaping Li, Chen Chen, and Dao Wen Wang

Supplemental Material

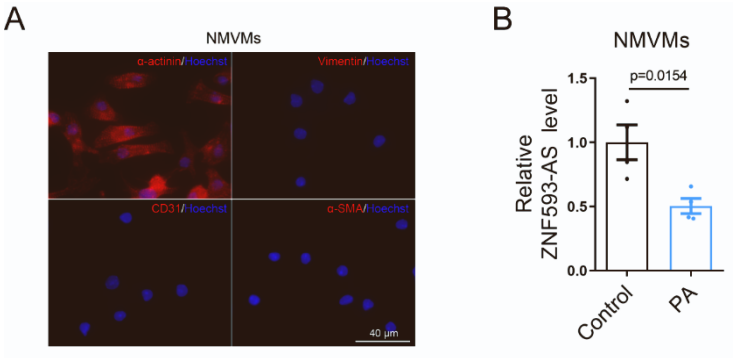

Figure S1. PA reduced ZNF593-AS level in NMVMs. (A) The purity of NMVMs indicated by immunofluorescence. (B) RT-qPCR analysis of ZNF593-AS levels in NMVMs under the stimulation of PA. Student's *t*-test was used for comparisons in (B).

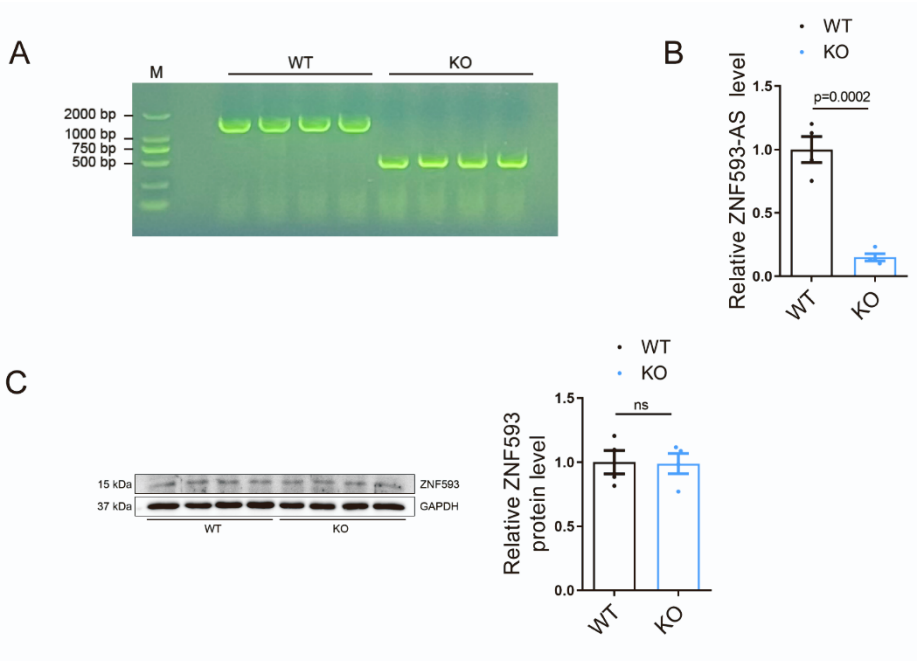

Figure S2. Genotyping of ZNF593-AS KO mice. (A) Genotyping of ZNF593-AS KO mice. (B) RT-qPCR analysis of ZNF-593-AS levels in ZNF593-AS KO mice hearts. (C) Western blotting analysis of ZNF593 protein levels in ZNF593-AS KO mice hearts. Student's *t*-test was used for comparisons in (B) and (C).

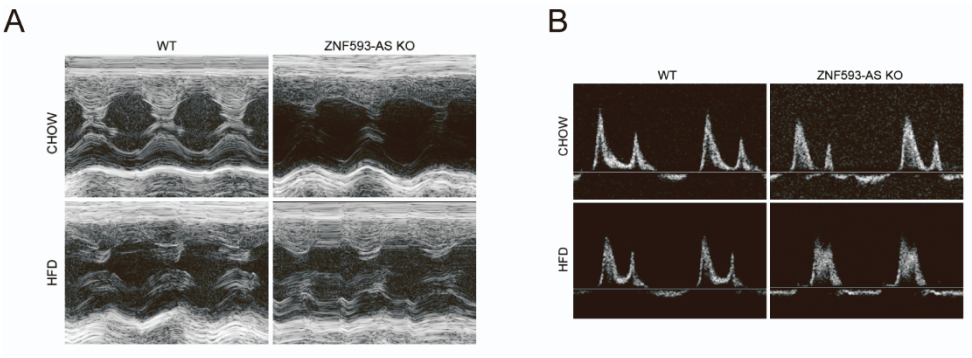

Figure S3. Representative images for M-mode and mitral valve flow of ZNF593-AS KO mice. (A) Representative images for M-mode of ZNF593-AS KO mice. (B) Representative images for mitral valve flow of ZNF593-AS KO mice.

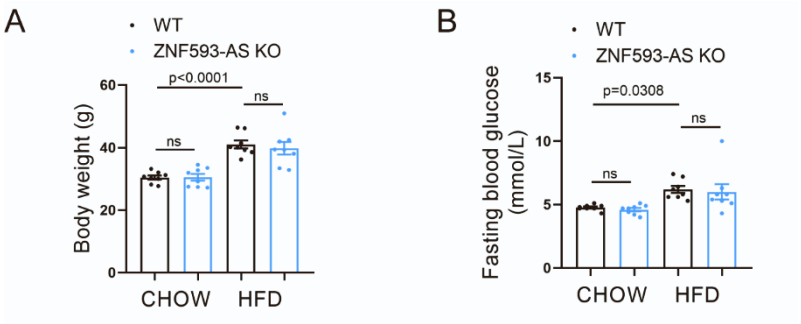

Figure S4. Body weight and fasting blood glucose were unaffected by ZNF593-AS deletion. (A and B) Body weight (A) and fasting blood glucose (B) of ZNF593-AS KO and WT mice fed with high-fat or normal diet. One-way ANOVA with the Tukey post-test was used (A) and (B).

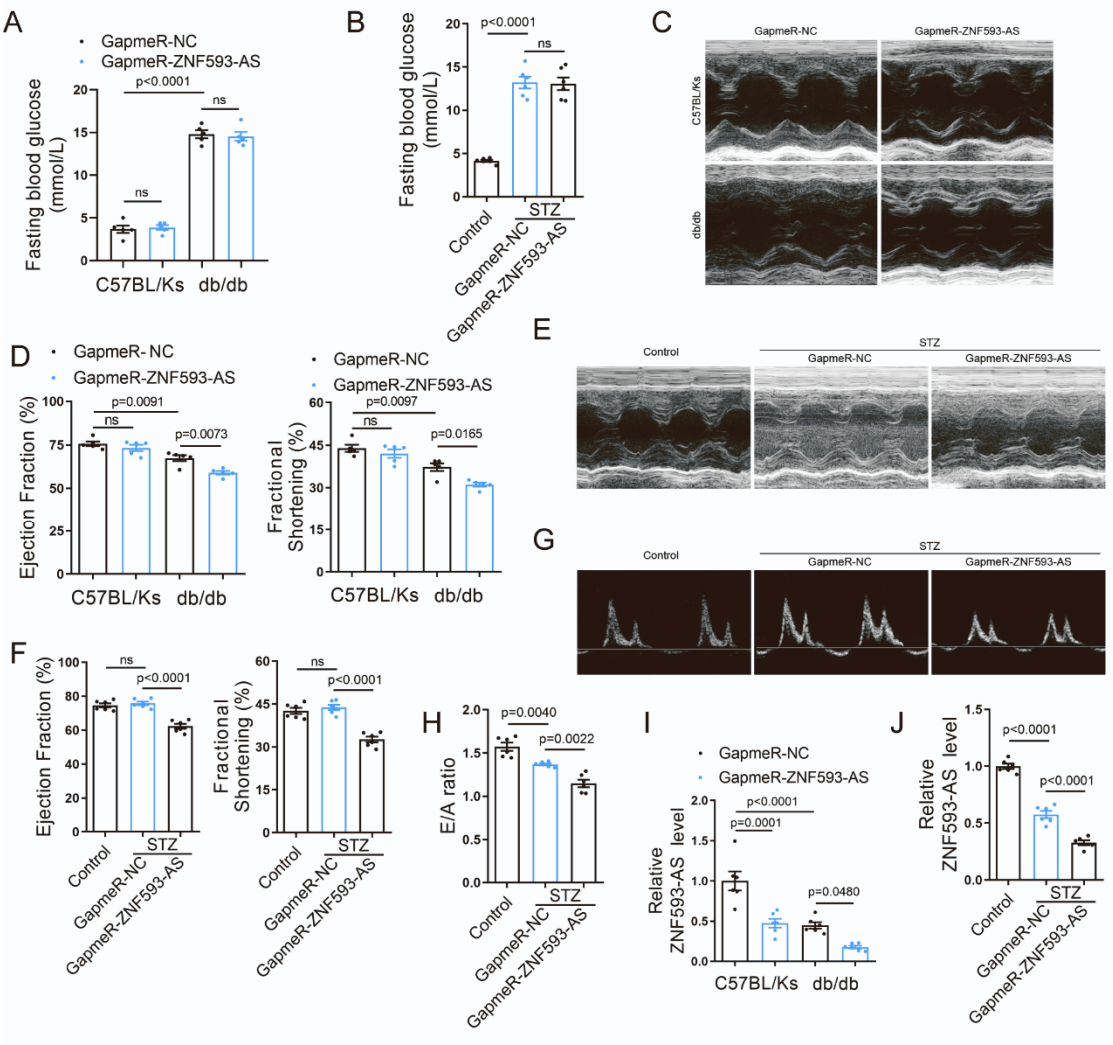

Figure S5. ZNF593-AS knockdown aggravated cardiac dysfunction in db/db and STZ-induced diabetic mice. (A) Fasting blood glucose of db/db and C57BL/Ks mice. (B) Fasting blood glucose of STZ-induced diabetic and control mice. (C) Representative images for M-mode of db/db and C57BL/Ks mice. (D) EF value and FS value of db/db mice and C57BL/Ks mice. (E) Representative images for M-mode of STZ-induced diabetic and control mice. (F) EF value and FS value of STZ-induced diabetic and control mice. (G) Representative images for mitral valve flow of STZ-induced diabetic and control mice. (H) E/A ratio of STZ-induced diabetic and control mice. (I) RT-qPCR analysis of the efficiency of ZNF593-AS knockdown in db/db mice hearts. (J) RT-qPCR analysis of the efficiency of ZNF593-AS knockdown in STZ-induced diabetic mice hearts. One-way ANOVA with the Tukey post-test was used (A), (B), (D), (F), (H), (I), and (J).

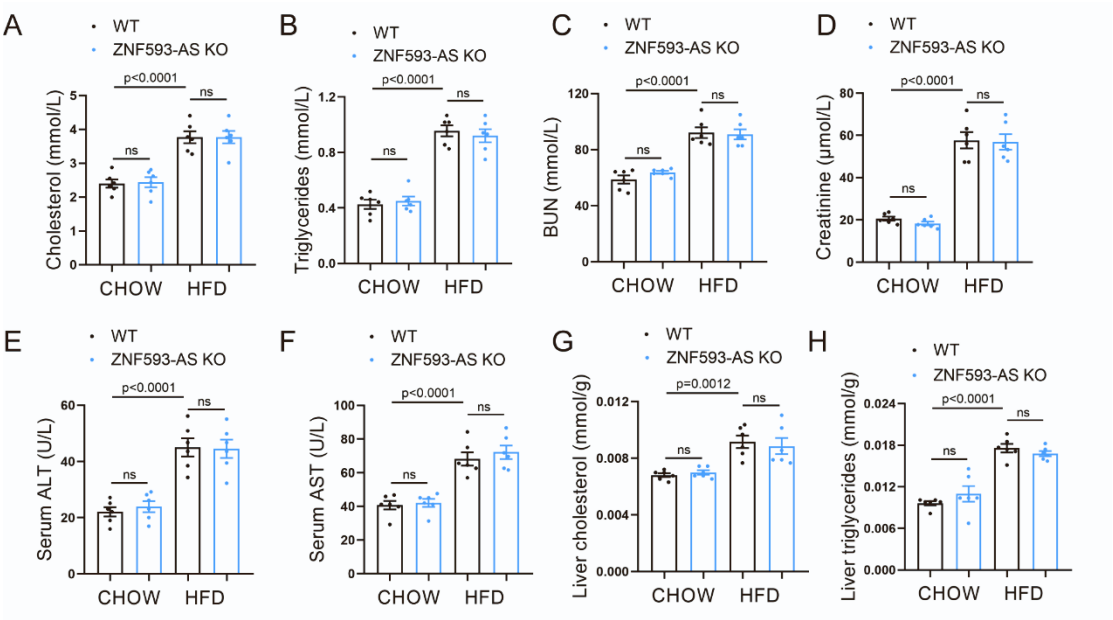

Figure S6. Serum biochemicals and hepatic metabolic parameters of ZNF593-KO mice. (A, B, C, D, E, and F) Circulating levels of cholesterol (A), triglycerides (B), urea nitrogen (BUN)(C), creatinine (D), alanine aminotransferase (ALT)(E), and aspartate aminotransferase (AST)(F) of ZNF593-AS KO mice. (G and H) Hepatic levels of cholesterol (G) and triglycerides (H) of ZNF593-AS KO mice. One-way ANOVA with the Tukey post-test was used (A), (B), (C), (D), (E), (F), (G), and (H).

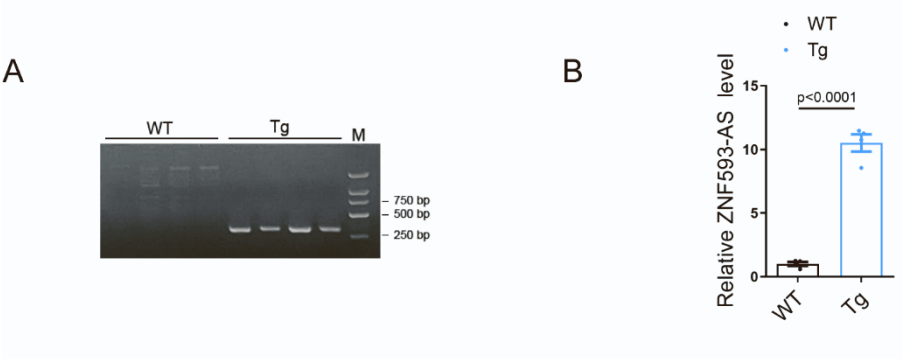

Figure S7. Genotyping of ZNF593-AS Tg mice. (A) Genotyping of ZNF593-AS Tg mice. (B) RT-qPCR analysis of ZNF593-AS levels in ZNF593-AS Tg mice hearts. Student's *t*-test was used for comparisons in (B).

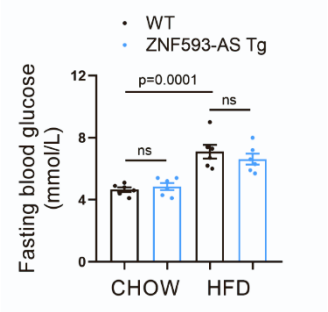

Figure S8. Fasting blood glucose of ZNF593-Tg mice. One-way ANOVA with the Tukey post-test was used for comparisons.

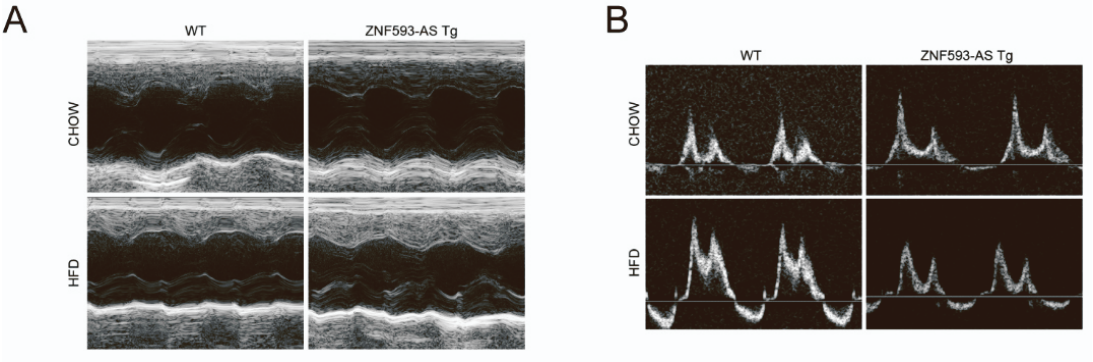

Figure S9. Representative images for M-mode and mitral valve flow of ZNF593-AS Tg mice. (A) Representative images for M-mode of ZNF593-AS Tg mice. (B) Representative images for mitral valve flow of ZNF593-AS Tg mice.

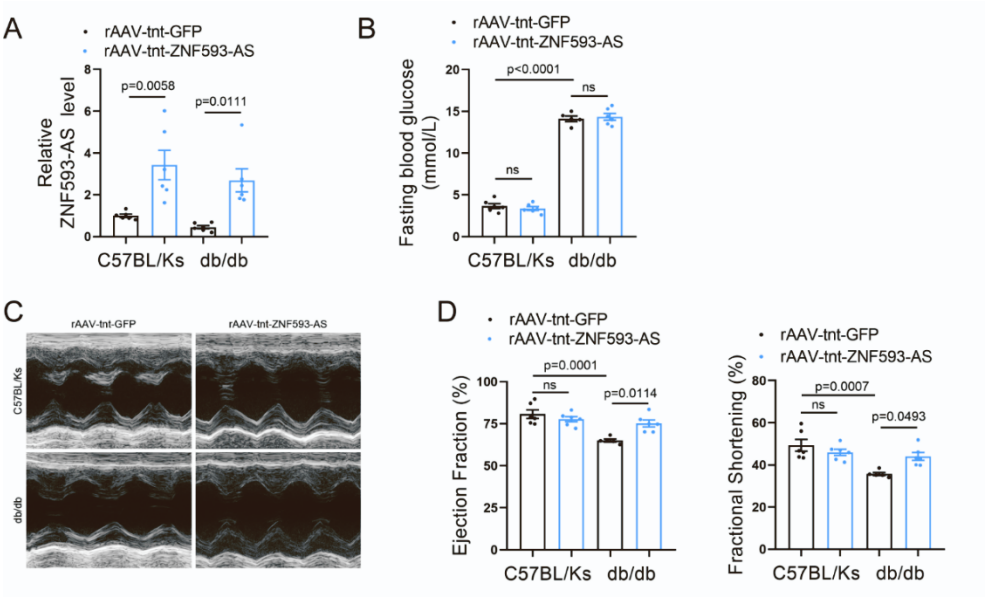

Figure S10. ZNF593-AS overexpression attenuated cardiac dysfunction in db/db mice. (A) RT-qPCR analysis of the efficiency of ZNF593-AS overexpression in the hearts of db/db and C57BL/Ks mice injected with rAAV9-tnt-ZNF593-AS or rAAV9-tnt-GFP. (B) Fasting blood glucose levels of db/db and C57BL/Ks mice. (C) Representative images for M-mode of db/db and C57BL/Ks mice. (D) EF value and FS value of db/db mice and C57BL/Ks mice. One-way ANOVA with the Tukey post-test was used in (A), (B) and (D).

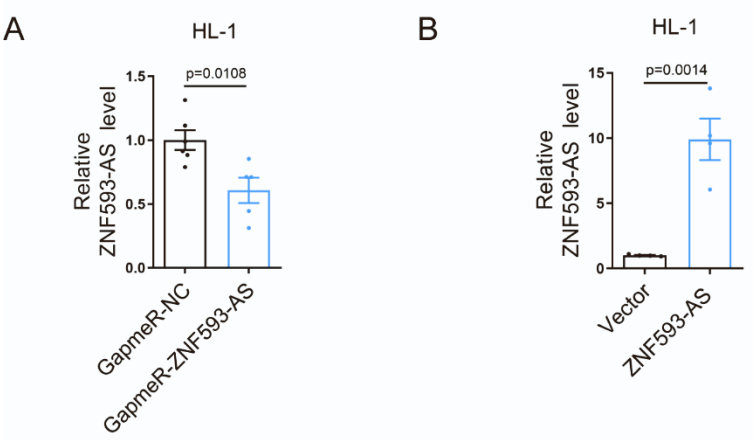

Figure S11. The efficiency of knockdown and overexpression of ZNF593-AS in vitro. (A) RT-qPCR analysis of the efficiency of ZNF593-AS knockdown in HL-1 cells. (B) RT-qPCR analysis of the efficiency of ZNF593-AS overexpression in HL-1 cells. Student's *t*-test was used for comparisons in (A) and (B).

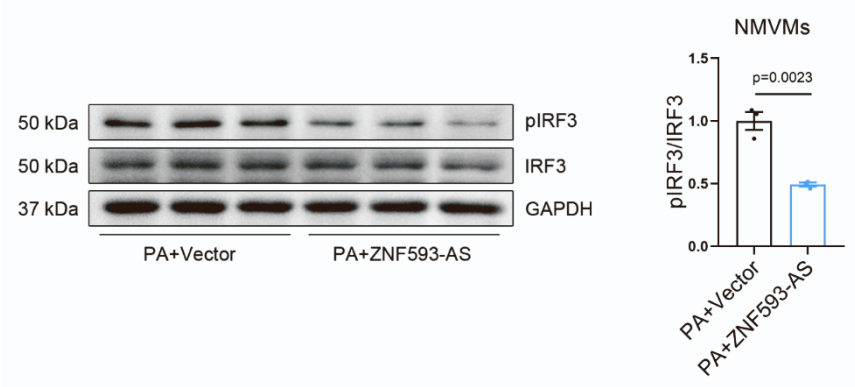

Figure S12. ZNF593-AS overexpression suppressed IRF3 phosphorylation in NMVMs. Student's *t*-test was used for comparisons.

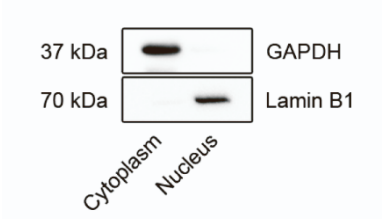

Figure S13. Determination of the purity of nuclear and cytoplasmic fractions. Western blotting analysis to determine the purity of nuclear and cytoplasmic fractions.

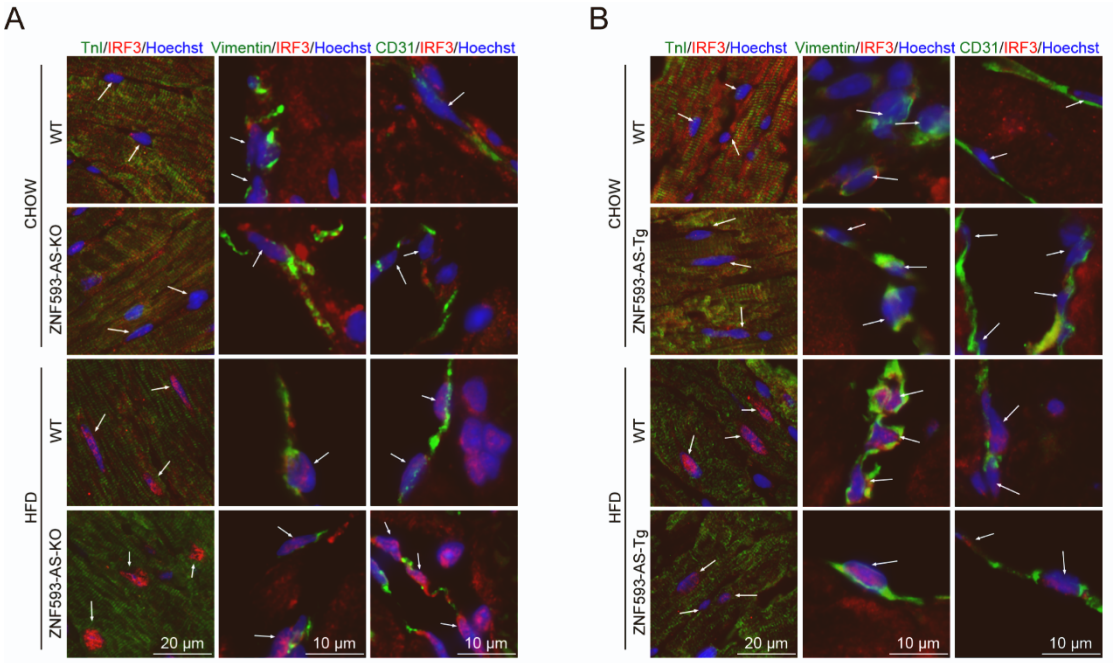

Figure S14. Co-staining IRF3 with different cardiac cell markers. (A and B) Co-staining IRF3 with different cardiac cell markers in ZNF593-AS KO (A) and ZNF593-Tg (B) mice heart.

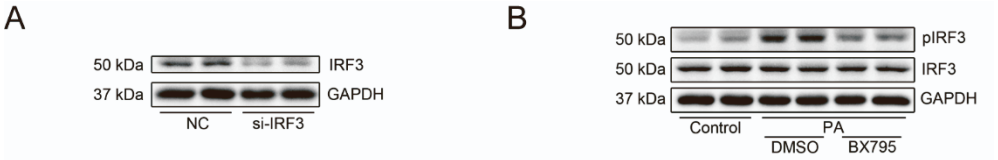

Figure S15. Inhibition of IRF3 signaling via knocking down IRF3 and suppressing IRF3 phosphorylation. (A) Western blotting analysis of the efficiency of IRF3 knockdown in HL-1 cells. (B) Western blotting analysis of phosphorylated and total IRF3 of BX795 treated HL-1 cells in the presence of PA.

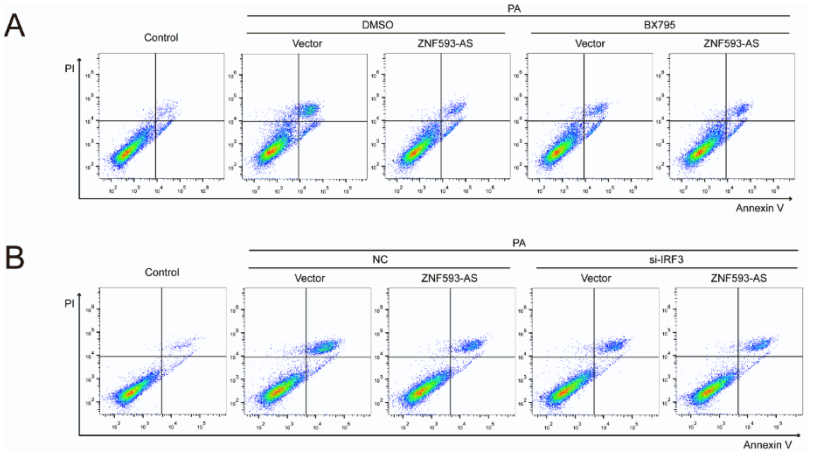

Figure S16. Representative flow cytometry dot plots for apoptosis analysis. (A and B) Representative flow cytometry dot plots for apoptosis analysis under BX795 treatment (A) and IRF3 knockdown (B).

Figure S17. The efficiency of IRF3 antibody to enrich IRF3 protein. (A and B) Western blotting analysis to validate the efficiency of IRF3 antibody to enrich IRF3 in HL-1 cells (A) and AC16 cells (B).

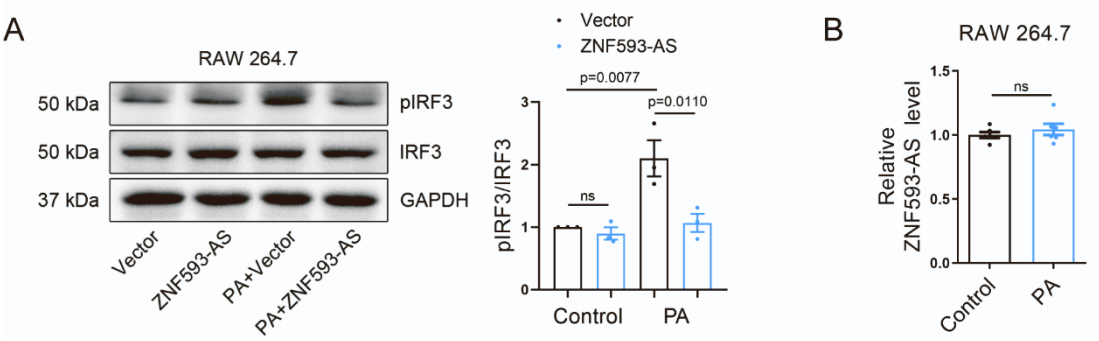

Figure S18. ZNF593-AS/IRF3 pathway in macrophage. (A) ZNF593-AS suppressed PA-induced IRF3 phosphorylation in RAW 264.7 cells. (B) RT-qPCR analysis of ZNF593-AS levels in RAW 264.7 under the stimulation of PA. One-way ANOVA with the Tukey post-test was used for comparisons in (A). Student's *t*-test was used in (B).

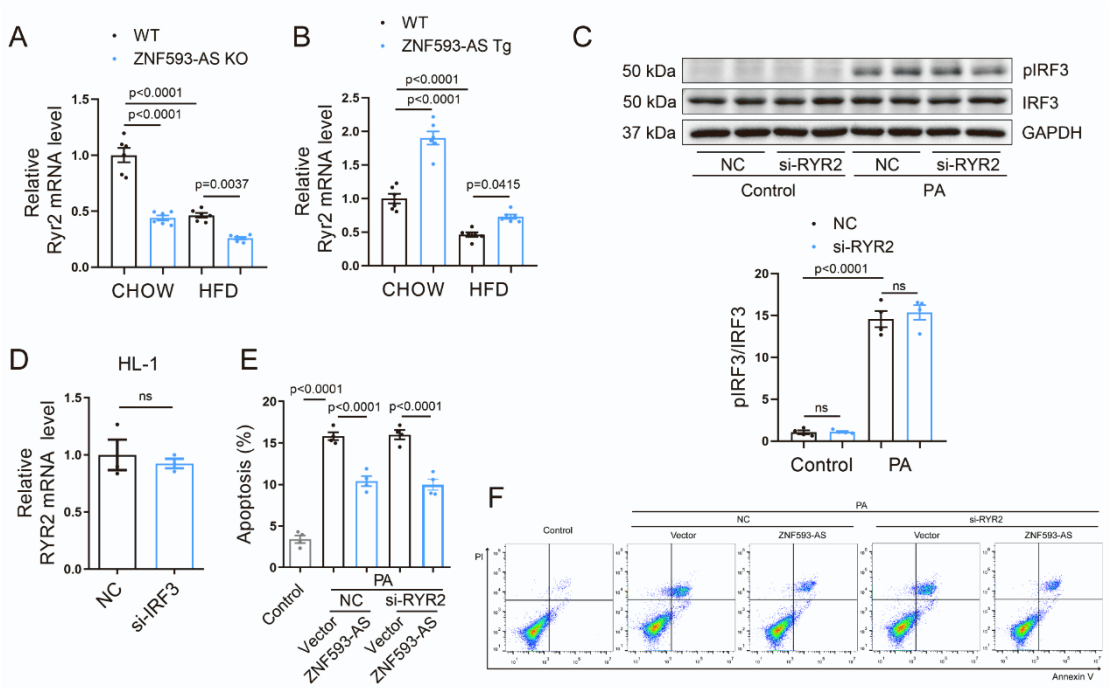

Figure S19. ZNF593-AS/RYR2 pathway in diabetic cardiomyopathy. (A) RT-qPCR analysis of RYR2 mRNA levels in ZNF593-AS KO mice hearts. (B) RT-qPCR analysis of RYR2 mRNA levels in ZNF593-AS Tg mice hearts. (C) RYR2 was unable to affect IRF3 phosphorylation. (D) IRF3 was unable to affect RYR2 expression. (E) RYR2 knockdown failed to diminish the anti-apoptotic effect of ZNF593-AS. (F) Representative flow cytometry dot plots for apoptosis analysis. One-way ANOVA with the Tukey post-test was used for comparisons in (A), (B), (C), and (E). Student's *t*-test was used in (D).

Table S1. Clinical characteristics of patients with chronic heart failure.

Patient	Gender	Age (years)	LVEF (%)	Diabetes mellitus
1	Male	62	37	No
2	Male	53	26	No
3	Male	47	30	No
4	Male	50	22	Yes
5	Male	68	31	Yes
6	Male	60	26	Yes
7	Male	66	22	Yes
8	Male	59	27	Yes

Table S2. List of PCR primers.

Primers	Forward 5'-3'	Reverse 5'-3'
h-ZNF593-AS	TGAGCACCCATCCATCAATCC	CCCAGGCAGCGCAGAGTCTT
m-ZNF593-AS	GGCTCCTGCTATGCAGTATGGA	TGGAGGGGTCAGTAGAGGACTG
m-Ifnb1	GATTGACGTGGGAGATGTCCTC	TCCTGAAGATCTCTGCTCGGAC
m-Cxcl10	GTGCTGCCGTCATTTTCTGC	TCCGGATTCAGACATCTCTGC
m-Ccl2	GCATCTGCCCTAAGGTCTTCAG	ACTGTCACACTGGTCACTCCT
m-Ccl5	CTCACCATATGGCTCGGACAC	TGGCGGTTCCTTCGAGTGAC
m-Ifit1	AGCAGAAGCACACATTGAAGAAG	TGCCAATTCTTGCACATTGTCCT
m-Oasl2	GCAAGCCTTTCACCATCGAC	TGAGTATGATGGTGTCGCAGTC
m-Isg15	GACGCAGACTGTAGACACGC	GCGCAAATGCTTGATCACTGT
m-Rsad2	AGAGGTGTCCTGTTTGGTGC	AGCTTCAGGTCAGCTTTACTCCA
m-Gapdh	GACCTCATGGCCTACATGGC	ATTATGGGGGTCTGGGATGGA
h-GAPDH	GACCCCTTCATTGACCTCAAC	CTTCTCCATGGTGGTGAAGA
18S rRNA	GTAACCCGTTGAACCCCATT	CCATCCAATCGGTAGTAGCG
m-Ryr2	CCTGCAAATGTGGAGGATGTCTG	CCACCTTGACATGTAGCTGCA